Journal Name

ARTICLE

Free ion diffusivity and charge concentration on cross-linked Polymeric Ionic Liquid iongels films based on sulfonated zwitterion salts and Lithium ions

Received 00th January 20xx,
Accepted 00th January 20xx

DOI: 10.1039/x0xx00000x

www.rsc.org/

David Valverde,[a] Abel Garcia-Bernabé,[b] Andreu Andrio,[a] Eduardo García-Verdugo,[a]* Santiago V. Luis,[a] Vicente Compañ*[b]

Abstract. The properties of a variety mixtures of a zwitterionic ionic liquid (**ZIs-1**) and $LiNTf_2$, including their conductivity, have been studied showing how they can be adjusted through their molar composition. Conductivity tends to increase with the $LiNTf_2$ content although presents a minimum at theregion close to the eutectic point. These mixtures also provide excellent features as liquid phases for the preparation of composite materials based on crosslinked PILs. The prepared films display excellent and tuneable properties as conducting materials, with conductivities that can be higher than 10^{-2} S cm^{-1} above 100 °C. The selected polymeric compositions show very good mechanical properties and thermal stability, even for low crosslinking degrees, along with a proper flexibility and good transparency. Final properties of the films correlate with the composition of the monomeric mixture used and with that of the **ZIs-1**:$LiNTf_2$ mixture.

Introduction

Lithium ion batteries have been considered as an attractive power source for a variety of wide applications such as consumer electronics, electric vehicles and energy storage systems.[1] Although these devices display good performance, polymer electrolytes are being explored as replacements for liquid electrolytes since they can maintain high ionic conductivities and good mechanical strengths without the risk of leakage and provide a larger operative temperature range.[2,3] Among these polymeric electrolytes, polymeric ionic liquids (PILs) have gained attention due to their interesting physical features in terms of their excellent thermal and chemical stability and ionic transport properties.[4] Nevertheless, the performance of PIL-based lithium ion batteries still needs to be improved in order to be fully competitive with those based on conventional systems.[5] In general, PILs show low conductivity values (~10^{-6} S cm^{-1}) as a result of the low mobility of the ionic moiety and have to be doped with ILs to form "ion-gels".[6] Since bulk ILs have high ion densities and high mobility of their component ions, they also provide a high ionic conductivity.[7,8] A particular class of ILs is that of *Zwitterionic ionic salts* (ZIs), having the cation and anion tethered in the same molecular structure.[9] ZIs do not display net charge and do not migrate even under a gradient of potential. ZIs can also interact with Li^+ or H^+ cations to obtain mixed molten salts. For instance, the addition of lithium bis(trifluoromethylsulfonyl)amide ($LiNTf_2$) or 1,1,1-trifluoro-N-(trifluoromethyl sulfonyl) methane sulfonamide ($HNTf_2$) to ZIs results in room temperature liquids due to the effects of the NTf_2^- anion.[10,11] Therefore, they are a good candidate to be used in combination with PILs to prepare advanced composite materials with potential applications in electrochemical devices such as lithium batteries or fuel cells.

In this paper, we demonstrated that different mixtures based on 3-(1-butyl-1H-imidazol-3-ium-3-yl)propane-1-sulfonate and $LiNTf_2$ mixtures can be used to develop stable "ion-gels" in PILs based on 1-methyl(-4-vynilbenzene)-3-butylimidazolium bis(trifluoromethylsulfonyl)imide (**IL-1**) and an appropriate crosslinking agent. The resulting films were analysed and characterised by impedance spectroscopy, DSC, TGA, ATR-FTIR and FT-Raman. The conductivity of the resulting films has been fully discussed and the free ion diffusivity and free ion charge density calculated and compared following two different procedures.

Results and Discussion

The zwitterionic salt **ZIs-1** (3-(1-butyl-1H-imidazol-3-ium-3-yl)propane-1-sulfonate) was obtained as previously reported by reaction of butylimidazole with 1,3-propanesultone as a white solid of high melting point (T_m = 170 °C, Fig S1).[7,9,10] Mixtures of this **ZIs-1** with different molar ratios of $LiNTf_2$ (Table 1) were obtained by solving both components in methanol, evaporation of the solvent and thorough vacuum drying or, better, they were prepared by mixing **ZIs-1** and $LiNTf_2$ in the solid state, in the ratios shown in Table 1, and heating the resulting mixture above the melting point of the . mixture. Mixtures containing a larger molar mass of $LiNTf_2$ ($x_{LiNTf_2} \geq 0.3$, from **M-1a** to **M-1d** and

[a] Dpto. Química Inorgánica y Orgánica, Universidad Jaume I, Avda. Sos, Baynat s/n, Castellon 12071, Spain..
[b] Dpto. de Termodinámica Aplicada, Universidad Politécnica de Valencia, C/Camino de Vera s/n, Valencia 46020, Spain

Electronic Supplementary Information (ESI) available: General experimental information and supplementary figures. See DOI: 10.1039/x0xx00000x

M-1g) were liquid at r.t., while those rich in the zwitterion salt ($x_{ZIs\text{-}1}$ > 0.7, **M-1e** and **M-1f**) were liquid-solid mixtures (Fig S2a).

Table 1. Composition of the mixtures based on **ZIs-1** and $LiNTf_2$

Entry[j]	M-1	Molar ratio[a]	$X_{ZIs\text{-}1}$	X_{LiNTf2}	State[b]	T_m[c]
1	**M-1a**	1:2	0.33	0.67	l	2
2	**M-1b**	1:3	0.25	0.75	l	9
3	**M-1c**	1:5	0.17	0.83	l	23
4	**M-1d**	2:1	0.67	0.33	l	16
5	**M-1e**	3:1	0.75	0.25	l-s	16
6	**M-1f**	5:1	0.83	0.17	l-s	16
7[d]	**M-1g**	1:1	0.5	0.5	l	**5**

[a] Molar ratio **ZIs-1**:$LiNTf_2$. [b] Solid (s) or liquid (l) state observed after drying under high vacuum till constant weight. [c] Calculated from the second cycle in DSC. [c] For the preparation and study of this mixture see ref. 11.

Those mixtures were also analysed by DSC and TGA (Figs S3-S4). DSC analysis confirmed the formation of a molten salt domain due to the plastic effect of the NTf_2 anion, with melting temperatures lower than the ones for the individual components. Mixtures **M-1a, M-1b, M-1c**, **M-1d** and **M-1g** (x_{LiNTf2} ≥ 0.3) showed melting temperatures lower than room temperature (Table 1 and Fig S3). Noteworthy the mixtures having a larger molar amount of **ZIs-1** and l-s original appearance (**M-1e** and **M-1f**) became also liquid at room temperature after heating at 240 °C. Indeed, the second DSC heating cycle of the mixtures showed only T_g values lower than 25 °C (Fig S3). TGA experiments also showed that **M-1e** and **M-1f** ($x_{ZIs\text{-}1}$ > 0.7) decomposed at similar temperatures than **ZIs-1** (*ca.* 320 °C), while mixtures with a larger amount of $LiNTf_2$ (x_{LiNTf2} ≥ 0.5) were stable up to *ca*. 360 °C.

The ^{1}H-NMR spectra of the mixtures in either CD_3OD or CD_3SOCD_3 did not show any significant shift for the signals characteristics of **ZIs-1** (Fig S2b) discarding the presence, in solution, of strong discrete interactions between the two components in solution. Noteworthy, however, the ATR-FTIR and Raman spectra of these mixtures provided important information on the nature of the interactions, in the pure mixtures, between **ZIs-1** and $LiNTf_2$,.[12] Fig 2 shows some selected regions of the spectra for **ZIs-1** and different **ZIs-1**:$LiNTf_2$ mixtures while the complete ATR-FT-IR spectra for the equimolecular mixture (**M-1g**) and the individual compounds (**ZIs-1** and $LiNTf_2$) have been included in the ESI (Fig S5). The peak assignable to the S-N-S asymmetric and symmetric stretching of the NTf_2, which appeared at 747 cm^{-1} at the lithium salt, was shifted in the mixture to lower wavenumbers (up to 740 cm^{-1}) suggesting a weaker interaction of Li^+ with this anion due to its additional coordination with the zwitterion. Indeed, the well-defined peaks assignable to the S-O stretching for **ZIs-1** at 755 and 749 cm^{-1} appeared in the mixture as broader signals shifted to higher frequencies. In a similar way, the strong band associated with the stretching vibration of the C-F group at 1061 cm^{-1} for $LiNTf_2$ was shifted to 1052 cm^{-1} in the mixture. The observed shifts are a function of the composition of the **ZIs-1**:$LiNTf_2$ mixture. Thus, for an increase from 0.5 to 0.83 in the molar fraction of $LiNTf_2$ the peak related to the S-N-S stretching shifts from 740 cm^{-1} to 744 cm^{-1} and the symmetrical stretching peak of the $–SO_2$-N-SO_2- from 1051 to 1057 cm^{-1}. Similar trends were found when the mixtures were analysed by Raman spectroscopy. The characteristic peak assignable to S-N-S stretching always appeared at lower wavenumbers in the mixtures, from 745 to 742 cm^{-1} as a function of the amount of **ZIs-1** (746 cm^{-1} for neat $LiNTf_2$, Fig S7). Changes were also observed for the bands of the imidazolium unit associated to the C(4)=C(5) and N(1)−C(2)−N(3) fragments, appearing in the Raman spectra of the mixtures at lower frequencies and as broader signals (*i.e.* 1445 cm^{-1} and 1419 cm^{-1} for **M-1a** in comparison with 1456 cm^{-1} and 1425 cm^{-1} for **ZIs-1**, see Fig S8). Similarly, the well-defined strong peak at 1561 cm^{-1} of **ZIs-1** shifts to 1565 cm^{-1} in **M-1a** experiencing a significant broadening and reduction of peak intensity. A related effect was also observed for the peaks appearing in the 1490-1380 cm^{-1} range, also attributed to imidazole ring vibrations. This clearly indicates a weakening of intramolecular interactions at the zwitterionic salt in the presence of $LiNTf_2$.[13]

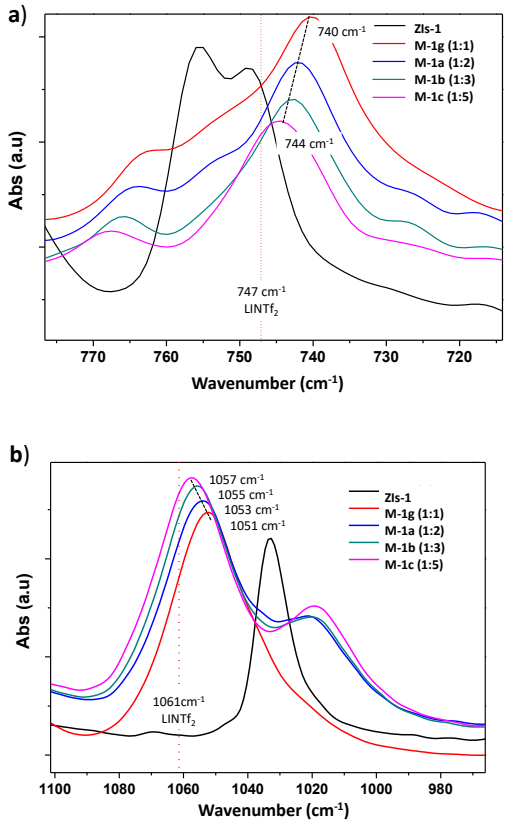

Figure 2 Selected regions of the ATR-FT-IR spectra of **ZIs-1** and **ZIs**:$LiNTf_2$ molar mixtures. The red line indicates the characteristic peak found for pure $LiNTf_2$.

A similar trend was also observed for the band at ~1250 cm^{-1} ascribed to the (S-O) stretching vibration (Fig S8). The peak shifts from 1242 cm^{-1} in bulk $LiNTf_2$ to lower frequencies with the presence of **ZIs-1** (1241, 1240 and 1239 cm^{-1} for **M-1c**, **M-1b** and **M-1a**, respectively). All these data suggest that in the mixtures the lithium cation is less coordinated to the NTf_2 anions.

The ionic conductivity of mixtures **M-1a, M-1b, M-1c**, **M-1d** and **M-1g** ($x_{LiNTf_2} \geq 0.33$) was measured (Fig 3). The measurement of the other mixtures was precluded as they were not fully liquid at room temperature. It is worth noting that the ionic conductivity of the pure zwitterionic salt (**ZIs-1**) was very low (below 10^{-8} S cm^{-2}),[14] while conductivities found for the mixtures were in the 10^{-2} to 10^{-6} S cm^{-1} range depending on the temperature and composition. The slightly convex curve observed in these plots for all the composites studied suggests that the ion conductive process can be expressed by the Vogel-Fulcher-Tamman (VFT) equation, describing the temperature dependence of viscosity in amorphous materials. Regarding the dependence with the composition (Fig S6), the equimolecular mixture (**M-1g**) led to the lowest conductivity, while the **ZIs-1**:$LiNTf_2$ mixture displaying a 1:5 molecular ratio (**M-1c**, x_{LiNTf_2} = 0.83) provided the highest conductivities for the temperatures assayed (*e.g.* 1.6 10^{-3}, 1.4 10^{-2} and 2.3 10^{-2} at 20, 80 and 100 ºC, respectively). As the **M-1d** mixture (x_{LiNTf_2} = 0.33) displayed always a conductivity higher than **M-1g**, it is clear that the concentration of $LiNTf_2$ is not the only factor determining the conductivity.

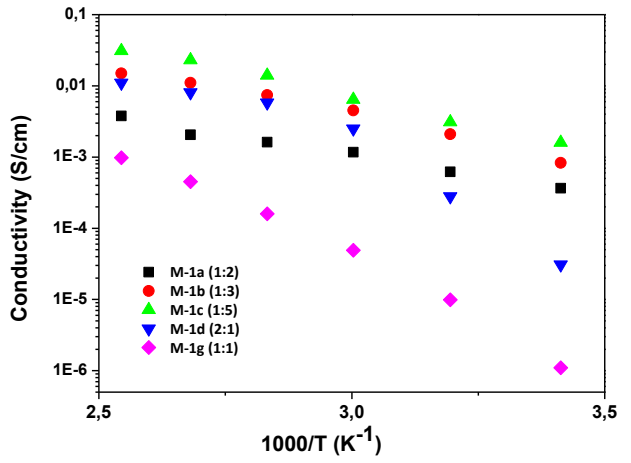

Figure 3. Ionic conductivity of the different **ZIs-1**:$LiNTf_2$ mixtures as a function of the temperature.

These differences on conductivity with the composition can be explained considering the concentration of the mobile ions and their mobility associated to the strength of the interactions between the species present in the mixtures and revealed by ATR-FTIR and Raman spectroscopy, as discussed above. In this context, physical properties like viscosity also relate to intermolecular and interionic interactions. At 25 ºC the viscosity increased with the $LiNTf_2$ content, except for the region close to the eutectic point for x_{LiNTf_2} = 0.67, where a minimum in viscosity is detected, following the expected trend for a eutectic mixture (Fig S6b). The measured viscosities were 123, 500, 49, 1090 and 2955 Pa·s for **M-1d**, **M-1g**, **M-1a**, **M-1b** and **M-1c**, respectively. At 100 ºC variations in viscosity are minimal, displaying values characteristic of non-viscous fluids, with the minimum value reached again at the eutectic point. Data presented in Fig. S6 show that conductivity also does not follow the expected trend of increasing conductivity when reducing viscosity. Instead, a constant increase in conductivity is observed for the higher $LiNTf_2$ contents (above the eutectic point) as a function of the concentration of the carrier, suggesting that near the eutectic point specific intermolecular interactions are present developing discrete supramolecular clusters (neutral net charge) that reduce ion mobility in spite of a reduced viscosity.

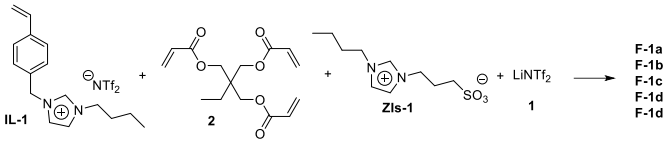

Scheme 1. Chemical composition of the films.

Cross-linked Polymeric Ionic Liquid ion-gel films. In the light of the excellent and tuneable conductivities achieved with the former mixtures composed by **ZIs-1** and $LiNTf_2$, a series of crosslinked polymeric films were prepared based on the mixtures displaying higher conductivities (and the equimolar mixture **M-1g**). This was carried out by polymerization of a crosslinking monomer (trimethylolpropane trimethacrylate, TMPTMA, **2**) and an ionic liquid monomer (**IL-1**) in the presence of the **ZIs-1**:$LiNTf_2$ mixtures (Scheme 1). Best results were obtained for the compositions shown in Table 2, providing mechanically stable and transparent films able to efficiently entrap the **ZIs-1**:$LiNTf_2$ mixtures inside the polymeric matrix without any sign of leaching even after several months of storage.[15,16] In these films, around 50% of the weight corresponds to the polymeric matrix and the other 50% to the **ZIs-1**:$LiNTf_2$ mixture.

Table 2. Films composition[a]

Film	PILs (wt %)[a]		ZIs-1:$LiNTf_2$[b]	Molar composition[c]		
	TMPTMA	IL-1		X_{IL-1}	X_{ZIs-1}	X_{LiNtf2}
F-1g'	10	90	**M-1g**	0,338	0,357	0,306
F-1g	5	95	**M-1g**	0,339	0,356	0,305
F-1a	5	95	**M-1a**	0,343	0,242	0,415
F-1b	5	95	**M-1b**	0,345	0,183	0,472
F-1c	5	95	**M-1c**	0,349	0,123	0,528

[a] Weight percentage of each monomer in the monomeric mixture. [b] 1:1 weight ratio with the monomeric mixture; for the composition of the **ZIs-1**:$LiNTf_2$ mixtures see Table 1. [c] Molar composition of the final films.

The five transparent, flexible polymeric films could be easily cut into any desired size and shape or be bent with one pair of tweezers, even under dry conditions. In these materials, two different components can contribute to their final conductivity: the ionic liquid fragment attached to the polymeric backbone derived from **IL-1** and the respective **ZIs-1**:$LiNTf_2$ mixture.
Differential scanning calorimetry (DSC) was used to determine the thermal properties of the obtained films. In the thermograms obtained at 10 K/min, under a nitrogen atmosphere, for the −50 - 275 C range (ESI, Fig S9) the non-doped polymeric films did not show any detectable T_g values for this temperature range. In the doped films, the transitions observed at low temperatures (*ca*. 5-20 ºC) correspond with

those for the isolated **ZIs-1**:LiNTf$_2$ mixtures (Fig S3). The TGAs of the films revealed their stability up to 350 ºC (Fig S10).

Regarding their conductivity, Figure 4 depicts the dependence of the dc-conductivity of the films doped with **ZIs-1**-LiNTf$_2$ mixtures with the temperature. Arrhenius behaviour was observed for the all composites. The activation energy follows the trend E_{act} (**F-1g'**) > E_{act} (**F-1g**)> E_{act} (**F-1a**) > E_{act} (**F-1b**) > E_{act} (**F-1c**) with the respective values being 22.8 ± 0.4, 21.3 ± 0.5, 19.8 ± 0.5, 19.7 ± 0.6 and 18.8 ± 0.7 kJ/mol.

The lower activation energy of **F-1g** in comparison with **F-1g'** can be correlated with the higher crosslinking degree of **F-1g'** (10% *vs* 5% of **2**). This is associated simultaneously to a reduced mobility of the polymeric chain and to a decrease in the loading of IL-like fragments covalently attached to the polymeric matrix. For the other films, having the same crosslinking degree, the E_{act} follows a lineal trend with the amount of LiNTf$_2$ (X_{LiNTf2}) present (Fig S11). Thus, the conductivity increases with X_{LiNTf2} following the trend observed in related **ZIs-1**:LiNTf$_2$ mixtures: $\sigma_{(F\text{-}1g)} \approx \sigma_{(F\text{-}1a)} < \sigma_{(F\text{-}1b)} < \sigma_{(F\text{-}1c)}$. The main contribution to the conductivity corresponds to the **ZIs-1**:LiNTf$_2$ mixtures, as the non-doped cross-linked films presented conductivities in the 10^{-5} to 10^{-10} range (**F-2** in Fig S12). The conductivity values obtained for the doped films were higher than those reported for related "ion-gel" cross-linked PILs containing either [BMIM][NTf$_2$] or [BMIM][Cl] (**F-3** and **F-4** in Fig S12). Thus, at 80ºC the conductivities were 4.8 x 10^{-3}, 5.1 x 10^{-3}, 7.2 x 10^{-3} and 9.8 x 10^{-3} S/cm for **F-1g**, **F-1a**, **F-1b** and **F-1c** (5.1 × 10^{-4} and 9.0 × 10^{-4} S/cm reported at the same temperature for **F-3** and **F-4**).[16]

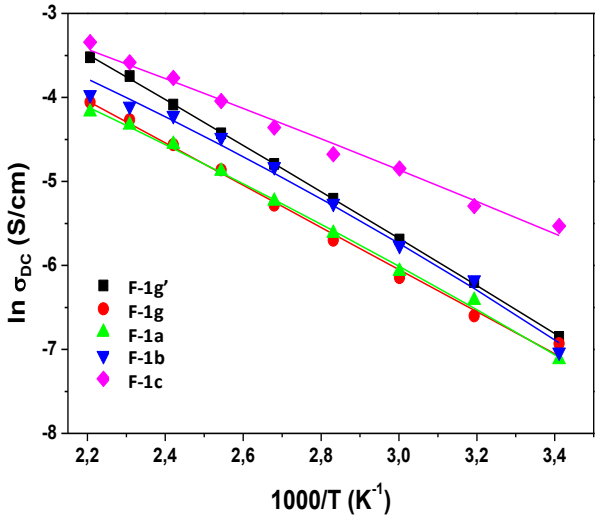

Figure 4 Temperature dependence of the dc-conductivity for the doped films.

ATR-FTIR and Raman spectroscopy provided again valuable information regarding the interaction of the charged ions in the composite materials, displaying similar trends to those observed in the related **ZIs-1**:LiNTf$_2$ mixtures. Thus, in the ATR-FTIR of the films, the symmetrical stretching peaks of the –SO$_2$ and the –SO$_2$–N–SO$_2$– groups appearing at 1198 cm^{-1} and 1060 cm^{-1} in neat LiNTf$_2$ were shifted to lower wavenumbers in the films (Fig S13). The shift was proportional to the **ZIs-1** content, reaching a frequency of 1178 cm^{-1} for **F-1g**. The characteristic Raman peaks for the NTf$_2^-$ anion, at 1241 and 746 cm^{-1} in the lithium salt, also appeared shifted to lower wavenumbers in the films (Fig S14) as a function of the **ZIs-1** content. Overall, the film **F-1c** having the larger loading of LiNTf$_2$ but still less associated ions than LiNTf$_2$ has the higher conductivity.

Diffusivity and ionic charge density. In order to get information about the behaviour of the ionic conductivity and diffusion processes for mobile carriers, electrochemical impedance spectroscopy measurements were performed on the different films.

The electrode polarization (EP) is a phenomenon which takes place always that a conductive sample is sandwiched between two electrodes. It is a consequence of the two interfaces formed between the two faces of the sample and the metallic phase of the electrodes. The polymeric film is a neutral matrix with a permittivity ε and thickness L sandwiched within two parallel plates of equal area. In the presence of an electric field, the free cation tends to accumulate near the negative electrode. The accumulation is limited by the concentration gradient and opposed to the electric force. In the time-dependent ac field, the ions at the interfaces depend on the time constant of the ac field. The application of an alternate electric field with angular frequency ω to a neutral matrix, produces a distribution of the charge into the polymeric matrix with an electrostatic double layer or Debye length L_D, given by the expression

$$L_D = \frac{1}{q}\left(\frac{\varepsilon \cdot k_B \cdot T}{n}\right)^{1/2}$$

where n is the charge concentration, k_B is the Boltzmann constant, ε the dielectric permittivity of the material and q the charge of a monovalent cation. Following the Coelho model, EP is found to be represented by a Debye relaxation for the characterization of the dielectric permittivity (ε*).[17] When the maximum in ε" corresponding to EP is difficult to separate from the conductivity, the procedure is to obtain the real and imaginary parts of the permittivity and the result is a simple equation for tan δ.[18] The application of the Cole-Cole relaxation for the description of electrode polarization given by eq. (1) can be used.

$$\varepsilon^*_{EP}(\omega) = \varepsilon_\infty + \frac{\Delta\varepsilon_{EP}}{1+(i\omega\tau_{EP})^\alpha} \quad (1)$$

Where

$$\Delta\varepsilon_{EP} = \varepsilon_{EP,s} - \varepsilon_\infty$$

is the strength of the relaxation, with the static permittivity in the presence of electrode polarization being

$$\varepsilon_{EP,s} = M\varepsilon_\infty,$$

α is a parameter related to the shape of the Cole-Cole relaxation and τ_{EP} is the electrode polarization time relaxation defined as

$$\tau_{EP} = M\tau = \frac{L}{2\mu}\left(\frac{\varepsilon}{nk_BT}\right)^{\frac{1}{2}} \quad (2)$$

being τ the relaxation time defined by

$$\tau = \frac{\varepsilon}{\sigma_{dc}}$$

and M the ratio of the sample thickness to twice the Debye length,

$$M = \frac{L}{2L_D} = \frac{qL}{2}\left(\frac{n}{\varepsilon k_BT}\right)^{1/2}$$

The real and imaginary parts of the Cole-Cole relaxation are respectively

$$\varepsilon'_{EP}(\omega)=\varepsilon_{\infty}+\frac{\Delta\varepsilon_{EP}\left[1+(\omega\tau_{EP})^{\alpha}\sin\left[\frac{\pi}{2}(1-\alpha)\right]\right]}{1+(\omega\tau_{EP})^{2\alpha}+2(\omega\tau_{EP})^{\alpha}\sin\left[\frac{\pi}{2}(1-\alpha)\right]}$$

$$\varepsilon''_{EP}(\omega)=\frac{\Delta\varepsilon_{EP}(\omega\tau_{EP})^{\alpha}\cos\left[\frac{\pi}{2}(1-\alpha)\right]}{1+(\omega\tau_{EP})^{2\alpha}+2(\omega\tau_{EP})^{\alpha}\sin\left[\frac{\pi}{2}(1-\alpha)\right]} \quad (3)$$

These equations can be fitted to the experimental data to provide values for ε, $\Delta\varepsilon_{EP}$, τ_{EP} and α, when the imaginary part shows a peak or shoulder with maximum at $f_{Ep}=1/(2\pi\tau_{EP})$.

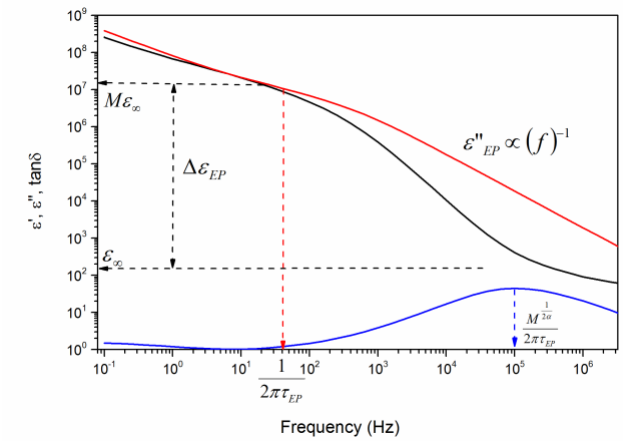

Figure 5. Dielectric permittivity (black), loss permittivity (red) and tan δ (blue) as a function of frequency for **F-1g'** at 20 °C.

When the conductivity term is very important, the imaginary part decreases with frequency increase with a slope close to minus one (-1), and the peak maximum is absent as can be observed in Figure 5 for **F-1g'**. In these cases, it is advisable to use eq. (3) adding the conductivity term $\sigma_{dc}/(\varepsilon_0\omega)$, in terms of

$$\tan\delta=\frac{\varepsilon''}{\varepsilon'}=\frac{\Delta\varepsilon_{EP}(\omega\tau_{EP})^{\alpha}\cos\left[\frac{\pi}{2}(1-\alpha)\right]+\frac{\sigma_{DC}}{\varepsilon_{vac}\omega}\left\{1+(\omega\tau_{EP})^{2\alpha}+2(\omega\tau_{EP})^{\alpha}\sin\left[\frac{\pi}{2}(1-\alpha)\right]\right\}}{\varepsilon_{\infty}\left\{1+(\omega\tau_{EP})^{2\alpha}+2(\omega\tau_{EP})^{\alpha}\sin\left[\frac{\pi}{2}(1-\alpha)\right]\right\}+\Delta\varepsilon_{EP}\left[1+(\omega\tau_{EP})^{\alpha}\sin\left[\frac{\pi}{2}(1-\alpha)\right]\right]} \quad (4)$$

The contribution of σ_{dc} can be removed for low conductivity values (< 10^{-5} S /cm) and when the maximum peak in tan δ is bigger than 100 Hz.[Error! Bookmark not defined.] The simplification can be used for very large values of M (M >>1). Under these conditions eq. (4) can be simplified to obtain

$$\tan\delta=\frac{(\omega\tau_{EP})^{\alpha}\cos\left[\frac{\pi}{2}(1-\alpha)\right]}{1+\frac{(\omega\tau_{EP})^{2\alpha}}{M}} \quad (5)$$

where the maximum in tan δ is verified for

$$\omega_{\max}^{\tan\delta}=\frac{M^{\frac{1}{2\alpha}}}{\tau_{EP}}=\frac{1}{\tau_m} \quad (6)$$

Where τ_m is the relaxation time associated to the conductivity. It is related with the frequency where tan δ shows a maximum. Notice that If α=1, then eqn (1) is reduced to Coelho model, where EP behavior is represented by a single Debye relaxation, and the eq.(6) is simplified to $\tau_{EP}=\tau_m\sqrt{M}$

The difference between the Cole-Cole and Debye descriptions is essentially the exponent α, that describes subdiffusion when $\alpha<1$. This exponent is the manifestation of cumulative processes in the system that are due to interactions among charge carriers. When $\alpha\ll1$ the interactions are strong, and when $\alpha\lesssim1$ the interactions do not dominate the transport process.

Taking into account the expression (2) together with M, the ionic mobility can be obtained as

$$\mu=\frac{qL^2}{4M^{1+\frac{1}{2\alpha}}\tau_m k_B T} \quad (7)$$

Knowing the mobility, the charge concentration is obtained from

$$n=\frac{\sigma_{dc}}{q\mu}=\frac{\sigma_{dc}4M^{1+\frac{1}{2\alpha}}\tau_m k_B T}{(qL)^2} \quad (8)$$

And the diffusivity considering to be related to mobility by means of the Nernst-Einstein equation,[19] will be

$$D=\frac{L^2}{4M^{1+\frac{1}{2\alpha}}\tau_m} \quad (9)$$

We can observe that eq(9) can be also easily obtained from the Macdonald-Trukhan model assuming identical diffusion coefficients for the anion, Da, and cation, Dc, (Da=Dc) where the average free ion difussivity, D, can be estimated as[19,22,23,24]

$$D=\frac{2\pi}{32}\frac{f_{\max}^{\tan\delta}\cdot L^2}{\left[(\tan\delta)_{\max}\right]^3} \quad (10)$$

Finally the static dielectric permittivity can be easily obtained to give

$$\varepsilon_{\infty}=\frac{\sigma_{dc}\tau_m}{M^{1-\frac{1}{2\alpha}}\varepsilon_{vac}} \quad (11)$$

Dielectric spectra results. The dielectric analysis of the composite materials considered can be illustrated using the complex permittivity, $\varepsilon^*(\omega,T)=\varepsilon'(\omega,T)-j\varepsilon''(\omega,T)$, where ε'(ω) and ε"(ω) are the real and imaginary parts of the frequency dependent permittivity due to the applied electric field, and j the imaginary unity ($j^2=-1$). The relation between the complex dielectric permittivity ε*(ω,T) and the complex conductivity, σ*(ω,T), is given by:

$$\sigma^*(\omega,T)=j\varepsilon_0\omega\varepsilon^*(\omega,T) \quad (12)$$

which can be decomposed in the real and imaginary parts as follows:

$$\sigma'=\varepsilon_0\omega\varepsilon'' \quad (13)$$

$$\sigma''=\varepsilon_0\omega\varepsilon' \quad (14)$$

where ε_0 represents the vacuum permittivity and ω the angular frequency of the applied electric field ($\omega=2\pi f$). The conductivity σ′ is characterized by a plateau regime that directly yields the dc conductivity. In this regime σ'(ω) is identical to the bulk dc conductivity σ_{dc} (*i.e.* σ_0). Typical curves showing the variation of the real part of conductivity for the films at different temperatures are shown in Figure 6.

In these graphics three different regions can be identified. The region at low frequencies, where the electrode polarization (EP)

effect produced by mobile charge accumulation from blocking electrodes is present,[20-27] the region where the dc-conductivity is dominant and will be determined by σ_{dc}, and the region at high frequencies where a subdiffusive conductivity (SD) is present, which may be due to the reorientation motion of dipoles and specifically to the motion of the localized charges, which dominates over the dc-conductivity.[18,21,28-30]

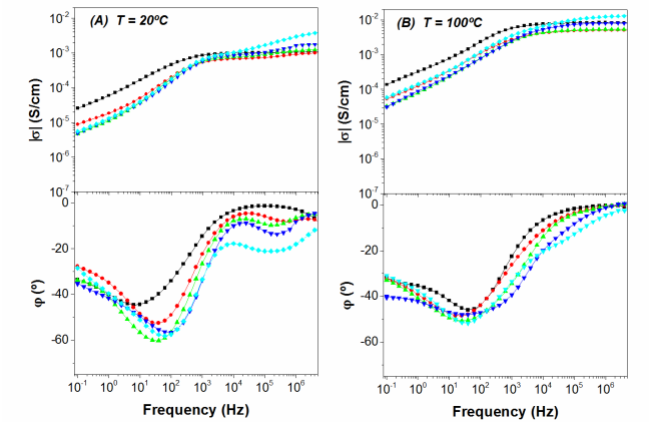

Figure 6. Bode diagrams for films **F-1g'** (black, squares), **F-1g** (red, circles) **F-1a** (green, up triangles), **F-1b** (blue, down triangles), **F-1c** (cyan, diamonds), at 20 and 100 ^{o}C. The conductivity and phase angle scales are the same in both temperatures for better comparison.

Figures 6A and 6B show the Bode diagrams for the different films at 20 and 100 ^{o}C, respectively. The top graphic represents the modulus of conductivity, $|\sigma|$, which increases with the frequency and tends to reach a constant value when the phase angle, φ (lower graphic), reaches a maximum or tend to a zero value for each temperature. It must be noted that the scales of conductivity are the same for both temperatures, which facilitates visualizing the variation of conductivity with temperature. As can be seen, all Bode diagrams showed a plateau when plotting $|\sigma|$ *vs* frequency in the region of high frequencies (10^3 Hz at 20 ^{o}C and 10^5 Hz at 100 ^{0}C), coexisting with the peak of the phase angles tending to zero values. On the other hand, in the region of high frequencies (10^4 Hz-10^7Hz at low temperatures, i.e.20 ^{o}C), a second plateau was observed for the conductivity of all samples except for the sample **F-1g'** at the region where the phase angle reaches a pronounced maximum around -10^{o}.

The presence of these two conductivities can be assigned to different processes related with the nature of the ions present in the polymeric matrix. Each ion can contribute in diverse ways to the motions within the material, depending on its shape, size and interaction with the polymeric matrix, providing different mobility and diffusion coefficients. It is important to bear in mind that the considered "ion-gels" have two different types of NTf_2^- anions, namely the counter ion of the polymeric ionic liquid-like imidazolium fragments and the NTf_2^- from $LiNTf_2$. On the other hand, the lithium cation (Li^+) can also contribute to the conductivity. It is likely that at least four possible transport events can add to the conductivity, all of them related with the mobility of the ions involving formation and breaking of ion-associations in the presence of an electric field (Scheme 2). The first one is related with the "free" intermolecular NTf_2^- hopping in the "ion-gel" phase. A second one should be the NTf_2^- hopping from the polymer to the liquid phase and vice versa. The third one is associated with the NTf_2^- hopping events along the polymeric chain. This one seems to be less important at the view of the low conductivity of the films in the absence of **ZIs-1**:$LiNTf_2$ mixtures. Finally, the events related with the mobility of "free" Li cations in the medium can also be considered, although the presence of the sulfonic groups in **ZIs-1** may constrain Li^+ mobility by complexation.

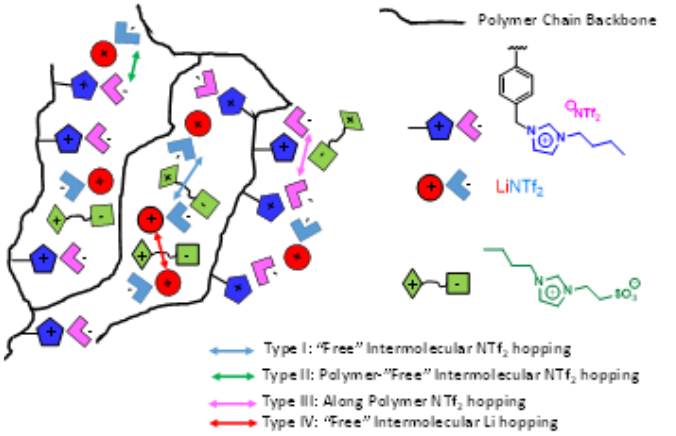

Scheme 2. Schematic representation of mobility events in the film.

In the different films considered, the NTf_2^- anion has two different origins, $LiNTf_2$ and the IL-like fragments from the polymerization of **IL-1**. In the last case, the mobility of the imidazolium cation is reduced as corresponds to its attachment to the polymeric backbone. The ratio between both anions changes systematically in the films. For instance, for **F-1g** the molar fraction of **IL-1** is very similar to the one of $LiNTf_2$ (0.339 and 0.305, respectively) leading to a total NTf_2^- : Li^+ ratio of 0.644 : 0.356. The progressive substitution in the mixtures of **ZIs-1** by the corresponding Li salt provides an increase in the molar fraction of $LiNTf_2$ that reaches, in the case of **F-1c**, a maximum value of 0.528. As the molar fraction of NTf_2^- in **F-1c** coming from **IL-1** in is 0.394, the overall NTf_2^- : Li^+ ratio is 0.877 : 0.528 in this film. This makes the total concentration of the NTf_2^- anion higher than the one for the Li^+ cation in all the films studied. Thus, the contribution to conductivity of the NTf_2^- anion is expected to be more pronounced than the one of Li^+. Previous studies carried out with films based on highly cross-linked PILs have also revealed the important contribution of the mobility of the anion to the measured conductivity.[15,16,31-33]

Journal Name

ARTICLE

Table 3. Parameters M, τ_{EP} and α described in equation (5) at 20, 60 and 100 °C, obtained from fitting the experimental data of tan δ

	T=20 °C			T=60 °C			T=100 °C		
Sample	M	τ_{EP} [s]	α	M	τ_{EP} [s]	α	M	τ_{EP} [s]	α
F-1g'	45000	3.5×10^{-4}	0.992	75000	1.2×10^{-4}	0.9975	100000	5.0×10^{-5}	0.9995
F-1g	5000	4.0×10^{-4}	0.970	11000	3.5×10^{-5}	1	300000	1.8×10^{-5}	1
F-1a	3000	3.8×10^{-4}	0.951	11000	2.5×10^{-5}	0.9999	-	-	-
F-1b	3000	4.0×10^{-4}	0.930	9000	1.4×10^{-5}	0.9990	-	-	-
F-1c	3300	7.0×10^{-4}	0.835	10000	6.5×10^{-6}	0.9920	-	-	-

Free ion diffusivity and charge concentration. The most important parameters to estimate the ionic transport in materials are the mobility and concentration of charge carriers and there are a great number of alternative approaches for determining these parameters under the application of an electric field.[18,19,34-54]

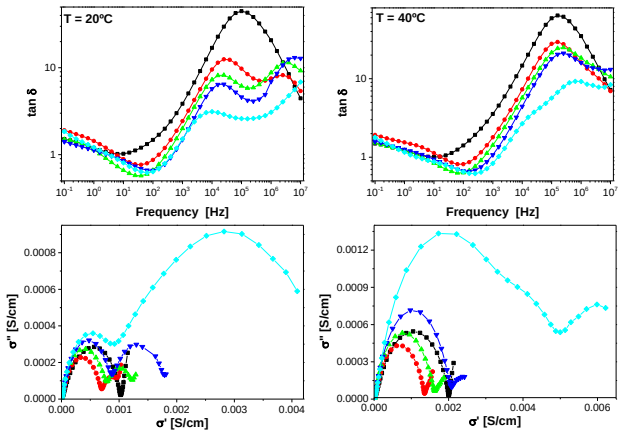

Figure 7. Tan δ as a function of frequencies (up) and Nyquist plots (bottom) at 20 °C (left) and 40 °C (right). **F-1g'** (■), **F-1g** (●), **F-1a** ( ), **F-1b** ( ), **F-1c** ( ).

Fig 7 shows the experimental values of *tan δ* for all samples at 20 and 40 °C obtained using a modification of the approach reported Klein *et al.*[15,16,18,22,23,31] As can be seen, the doped films, except **F-1g'** presenting a higher crosslinking degree, present two clear peaks around 10^4 Hz and between 10^6-10^7 Hz, respectively, at 20 °C. The peak at moderate frequencies (10^4 Hz to 10^5Hz) is shifted towards higher frequencies as the temperature increased bringing both peaks together. Similarly, the same behaviour is observed from the Nyquist diagrams showed in Fig.7 (bottom) where at 20ºC two semicircles are present due presumable to two types of mobilities and conductivities also observed in the Bode diagrams.

In a first approach, the tan δ values for the detected maxima in Fig 7 were fitted to eq. (5). This provided an estimation for M, τ_{EP} and α, and also allowed calculating the free ion diffusivity. Values obtained for α were close to unity, indicating a limit value in the Cole-Cole model corresponding to a Debye behaviour. A dependence on the temperature of the electrode polarization relaxation time τ_{EP} and the parameter M, was also observed.

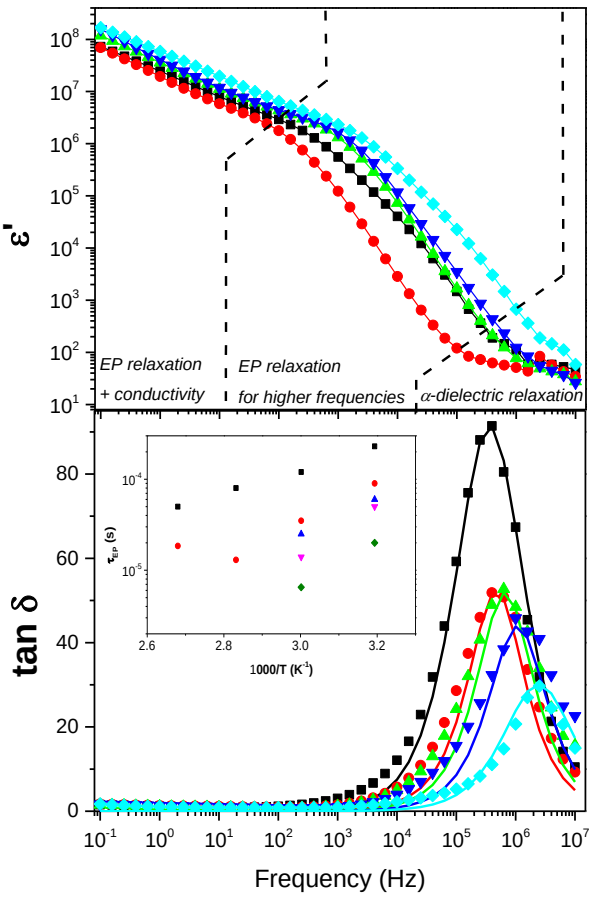

Figure 8. Dielectric permittivity (top) and *tan δ* (bottom) as a function of frequencies at 60 °C. **F-1g'** (■), **F-1g** (●), **F-1a** ( ), **F-1b** ( ) and **F-1c** ( ). The solid line indicates the convolution of equation 11 in the peak of *tan δ* at higher frequencies. The insert displays is the temperature dependence of τ_{EP}.

The curves shown in Fig 8 display the peaks corresponding to the maximum in tan δ (Eq. (5)) and are associated with the plateau of the real part of the conductivity observed in the Bode diagrams (Fig 6). Their corresponding values in frequency are related with the parameters M, α and τ_m, which permits to calculate the mobility, the ionic diffusion coefficient and the density of free charge into the polymeric matrix applying eqs. (7), (8) and (9), respectively.

Fig 8 also shows the dielectric permittivity and the temperature dependence of τ_{EP} is presented in the inset. A dielectric α-relaxation effect can be observed in tan δ spectra with an excess wing at higher frequencies and as a jump in dielectric spectra. After EP relaxation, a decrease in dielectric permittivity appears in dielectric spectra until reaching constant value in the range of high frequencies, although for some samples the expected plateau is not still visible at the experimental frequencies used. Table 3 summarizes the parameters for the analysis of eq. (5) at 20, 60 and 100 °C, respectively. A close inspection of Table 3 shows that parameters M and τ_{EP} decrease as the amount of $LiNTf_2$ increase in the film, with the highest value being always obtained for **F-1g'** with a higher crosslinking degree.

The temperature dependence of τ_{EP} exhibits an essentially linear behaviour for the range of temperatures analysed. Diffusion coefficients, dielectric permittivity (static permittivity) and mobile charge concentration were calculated using eqs. (7)-(10) and are shown in Fig. 9. The values for the diffusion coefficients are reasonably similar to those for other related systems,[15,16,33,37] and increase with temperature increase. A close inspection of the variation of the values represented in the activation plot of Fig.9 allows indicates the excellent ion mobilities that can be obtained with these films. The comparison between them reveals that a decrease in the crosslinking degree **F-1g'** and **F-1g** associated with practically the same amount of IL produce a decreasing of the diffusion coefficient between one or two order of magnitude depending of the temperature. For the others films the diffusivity increase with the amount of NTf2-.

The calculated charge concentration increases with temperature and varies for the five films, being higher, rather surprisingly, for **F-1g'** and lower for the other films, correlating with the amount of ZIs-1 present in the film.

On the other hand, the values of the mobile ion concentration are higher than those from stoichiometric calculations providing a total concentration of ions (n_{tot}) around 10^{27} m^{-3} at room temperature. This yields a dissociation degree of roughly 10^{-2} at 20 °C. These values are quite similar to those found for other polyelectrolytes like a Li^+ poly(ethyleneoxide)-based sulfonated ionomer.[18] Thus, it seems that the analysis based on electrode polarization sub estimates ion diffusivity respect the estimation from Einstein relation, (D^*), considering the stoichiometric free-ion number density, where $D^*=\sigma_{dc}\, k_BT/n\, q^2$. It is due because in Einstein equation the number density of free ions, (n_{tot}), is considered complete and then it is constant for any temperature. However the dissociation-association dynamics should be assumed to be much faster than the macroscopic electrode polarization and increasing with the temperature.

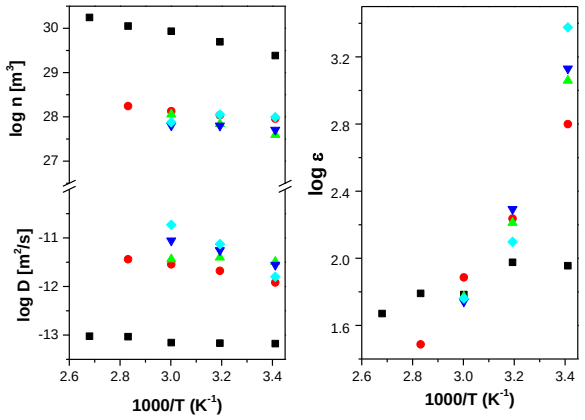

Figure 9. (Left) Temperature dependence of free ion diffusion (D) and charge concentration (n), (Right) dielectric permittivity (ε) for the films. **F-1g'** (■), **F-1g** (●), **F-1a** ( ), **F-1b** ( ), **F-1c** ( ).

In general, the free ion concentration can be described by the Arrhenius equation

$$n=n_0 \exp(-E_{dis}/k_BT)$$

where E_{dis} is the dissociation energy and n_0 the number density in the high temperature limit at which a complete dissociation can be assumed. The values found for the dissociation energy of the different samples were E_{dis} (**F-1g'**) = 9.5 kJ/mol > E_{dis} (**F-1a**) = 9.4 kJ/mol > E_{dis} (**F-1g**)= 4.0 kJ/mol > E_{dis} (**F-1c**)= 2.2 kJ/mol > E_{dis} (**F-1b**)= 2.0 kJ/mol. This energy increases with the value of X_{ZIs}. As it is known, the electrode polarization model is based on the Debye-Hückel theory and therefore can be expected that this model fails in the case of high ionic concentrations.

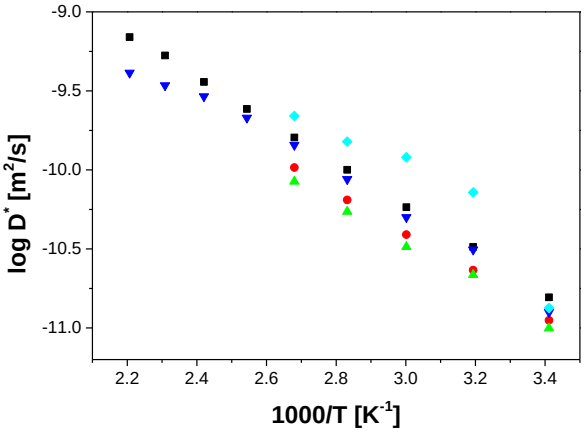

Figure 10. Temperature dependence of the corrected diffusion coefficient of the free ions for all the samples. **F-1g'** (■), **F-1g** (●), **F-1a** ( ), **F-1b** ( ), **F-1c** ( ).

A comparison between the values of the diffusion coefficients obtained from EP model and using the Einstein relation suggests a possible correlation between the conductivity and the increase in free charge carrier density. This can be due to structural and morphological changes occurring at the ILs phase and at the polymeric matrix. Figs 9 and 10 show that in general the diffusivity (*i.e.* mobility) increase with increasing temperatures that can also contribute to increase the

concentration of charge carriers and/or the conductivity. This trends can be associated with the variations in interionic interactions that will be higher with an increase in loading of functional groups in the polymer, with an increase in the concentration of IL-phase that could facilitate such interactions, most likely through an array of polar species, and with an increase in temperature that will favour the mobility of the polymer chains bearing the functional sites. In this regard, an increase in the amount of crosslinker (TMPTMA) decreases the diffusivity as it reduces polymer chain mobility and accordingly interactions between ions in the liquid phase and those covalently attached to the polymer matrix. This is illustrated in Fig 10 by the comparison between **F-1g** and **F-1g'**. Interestingly, the same figure shows that these two films prepared with a 1:1 **ZIs-1**:$LiNTf_2$ mixture (in the region of the eutectic point) are the only ones displaying a diffusivity that increases with temperature as corresponds with the presence of discrete clusters in the eutectic and a limited number of long-range cluster-cluster interactions in the eutectic. It is known that ionic mobility is associated and coupled to structural relaxation and high ionic conductivity is possible due to very short structural relaxation time such is happen in our samples, $\tau \approx 10^{-6}$ s, where the polymer have relatively rigid structures and then the ionic transport can be strongly decoupled from the structural relaxation.

Conclusions

The results presented here show that the properties of the mixtures of the zwitterionic imidazolium salt **ZIs-1** with $LiNTf_2$ can be tuned through a proper selection of the molar fraction of both components. Changes in the composition define not only the concentration of mobile ions but also the strength of the interactions between anions and cations that affect their mobility and macroscopic properties like viscosity and finally conductivity, which is affected by a balance between all those factors. Thus, mixtures in the eutectic point show the lower conductivities that increase significantly for the higher contents in $LiNTf_2$. The incorporation of those mixtures into crosslinked polymeric matrices allows obtaining composite materials with excellent properties and potential for devices requiring conductive membranes, with no leaching of the liquid phase observed after long term experiments. The conductivity of the different films prepared increases with temperature and with the content in $LiNTf_2$, reaching maximum values for **F-1c** (i.e. 2.0×10^{-2} S cm^{-1} at 140 °C). These conductivity values indicate that such composite materials represent a promising alternative for application in different energy devices. It must be noted that **F-1c** presents an excellent mechanical and thermal stability, even for small crosslinking degrees, while being flexible and transparent. A further increase in the amount of $LiNTf_2$, however, did not allow obtaining films with the required properties. The comparison of **F-1g** and **F-1g'** shows that a moderate increase in crosslinking (from 5 to 10% of TMPTMA) is accompanied in this case by a slight increase in conductivity (i.e. 9.7×10^{-3}. *vs*. 1.6×10^{-2} S cm^{-1} for **F-1g** and **F-1g'** respectively) with activation energies associated of 22.8 and 21.3 kJ/mol, respectively

Although the study of free ion diffusivity and number density from the EP model gives reasonable estimates, the direct quantitative data need to be handle with some caution. Our results indicate that this approach tend to overestimate the values of mobile charge density (n) and, therefore, to underestimate the values of the diffusion coefficients (D). This can be solved, using the same line of reasoning developed by Wang *et al.*,[24,37] through the use of the corrected diffusion coefficient (D^*) calculated using the ratio between the stoichiometric charge density and the one calculated using the EP model

$$N = \frac{n_{tot}}{n_0}.$$

This means that overestimation of ion of mobile charge density is a generic problem in electrode polarization analysis, which may be originated from the estimation of the ionic carriers density, from the definition of conductivity and the Eisntein relation, because in such consideration the free ion number density should be considered constant with temperature, although this parameter (n) can increase by about 10^3-10^4 with the temperature. Consequently, the diffusion coefficient obtained from EP model decreases with temperature in comparison with that obtained directly by means of the Einstein relation considered constant to the number of ionic carriers.

Conflicts of interest

There are no conflicts to declare.

Acknowledgements

Financial support has been provided by MINECO (ENE/2015-69203-R) and Generalitat Valenciana (PROMETEO/2016/071). Technical support from the SECIC of the UJI is also acknowledged. DV thanks UNED (Costa Rica) for a predoctoral fellowship.

Notes and references

1 V. Etacheri, R. Marom, R. Elazari, G. Salitra and D. Aurbach, *Energy Env. Sci.,* 2011, **4**, 3243.
2 A. Arya and A. L. Sharma, *Ionics*, 2017, **23**, 497.
3 J. Kalhoff, G. G. Eshetu, D. Bresser and S. Passerini, *ChemSusChem*, 2015, **8**, 2154.
4 A. Eftekhari, Y. Liu and P. Chen, *J. Power Sourc.*, 2016, **334**, 221.
5 I. Osada, H. de Vries, B. Scrosati and S. Passerini *Angew. Chem. Int. Ed.*, 2016, **55**, 500.
6 A. S. Shaplov, R. Marcilla and D. Mecerreyes, *Electrochim. Acta*, 2015, **175**, 18.
7 M. Yoshizawa, M. Hirao, K. Ito-Akita and H. Ohno, *J. Mater. Chem.*, 2001, **11**, 1057.
8 M. Watanabe, M. L. Thomas, S. Zhang, K. Ueno, T. Yasuda and K. Dokko, *Chem. Rev.*, 2017, **117**, 7190.
9 M. Yoshizawa, A. Narita and H. Ohno, *Aus. J. Chem.*, 2004, **57**, 139.
10 M. Yoshizawa and H. Ohno, *Chem. Commun*., 2004, 1828.
11 M. Yoshizawa-Fujita, T. Tamura, Y. Takeoka and M. Rikukawa, *Chem. Commun.,* 2011, **47**, 2345.
12 V. H. Paschoal, L. F. O. Faria and M. C. C. Ribeiro, *Chem. Rev.*, 2017, **117**, 7053.

13 A. Narita, W. Shibayama and H. Ohno, *J. Mater. Chem.*, 2006, **16**, 1475.
14 H. Ohno, M. Yoshizawa-Fujita and Y. Kohno, *Phys. Chem. Chem. Phys.*, 2018, **20**, 10978.
15 A. Garcia-Bernabé, A. Rivera, A. Granados, S. V. Luis and V. Compañ, *Electrochim. Acta,* 2016, **213**, 887.
16 B. Altava, V. Compañ, A. Andrio, L. F. del Castillo, S. Mollá, M. I. Burguete, E. García-Verdugo and S. V. Luis, *Polymer*, 2015, **72**, 69.
17 R. Coelho, *J. Non-Cryst. Solids*, 1991, **131**, 1136.
18 R. J. Klein, S. Zhang, S. Dou, B. H. Jones, R. H. Colby and J. Runt. *J. Chem. Phys.*, 2006, **124**, 144903. See eq. (A5)
19 T. M. W. J. Bandara, M. A. K. L. Dissanayake, I. Albinsson and B. E. Mellander, *Solid State Ionics*, 2011, **189**, 63.
20 U. H. Choi, A. Mittal, T. L. Price, H. W. Gibson, J. Runt and R. H. Colby, *Macromolecules*, 2013, **46**, 1175.
21 A. Serghei, M. Tress, J. R. Sangoro and F. Kremer, *Phys. Rev. B*, 2009, **80**, 184301.
22 T. S. Sorensen, V. Compañ and R. Díaz-Calleja. *J. Chem. Soc. Faraday Trans.*, 1996, **92**, 1947.
23 T. S. Sorensen and V. Compañ. *J. Chem. Soc. Faraday Trans.*, 1995, **91**, 4235.
24 Y. Wang, F. Fan, A. L. Agapov, T. Sait, J. Yang, X. Yu, K. Hong, J. Mays and A. P. Sokolov, *Polymer*, 2014, **55**, 4067.
25 C. Krause, J. R. Sangoro, C. Iacob and F. J. Kremer, *Phys Chem. B*, 2010, **114**, 382.
26 D. Fragiadakis, S. Dou, R. H. Colby and J. Runt, *J. Chem. Phys.*, 2009, **130**, 064907.
27 D. Fragiadakis, S. Dou, R. H. Colby and J. Runt, *Macromolecules*, 2008, **41**, 5723.
28 J. Leys, M. Wübbenhorst, C. P. Menon, R. Rajesh, J. Thoen, C. Glorieux, P. Nockemann, B. Thijs, K. Binnemans and S. Longuemart, *J. Chem Phys.*, 2008, **128**, 064509.
29 J. R. Sangoro, A. Serghei, S. Naumov, P. Galvosas, J. Karger, C. Wespe, F. Bordusa and F. Kremer, *Phys. Rev. E.*, 2008, **77**, 051202.
30 A. Munar, A. Andrio, R. Iserte and V. Compañ, *J. Non-Cryst Solids*, 2011, **357**, 3064.
31 A. Garcia-Bernabé, V. Compañ, M.I. Burguete, E. García-Verdugo, N. Karbass, S. V. Luis and E. Riande. *J. Phys Chem C*, 2010, **114**, 7030.
32 V. Compañ, S. Molla, E. García-Verdugo, S. V. Luis and M. I. Burguete, *J. Non-Cryst. Solids*, 2012, **358**, 1228.
33 B. Huber, L. Rossrucker, J. Sundermeyer and B. Roling, *Solid State Ionics*, 2013, **247-248**, 15.
34 A. S. Shaplov, R. Marcilla and D. Mecerreyes, *Electrochim. Acta*, 2015, 175, 18.
35 M. D. Green, D. Wang, S. T Hemp, J. H. Choi, K. I. Winey, J. R. Heflin and T. E. Long, *Polymer*, 2012, **53**, 3677.
36 V. Compañ, T. S. Sorensen, R. Díaz-Calleja and E. Riande, *J. Appl. Phys.*, 1996, **79**, 403.
37 Y. Wang, C.-N. Sun, F. Fan, J. R. Sangoro, M. B. Berman, S. G. Grenbaum, T. A. Zawodzinski and A. P. Sokolov, *Phys. Rev. E.*, 2013, **87**, 042308.
38 J. R. MacDonald, *J. Phys. Condens. Matter*, 2010, **22**, 495101.
39 J. R. MacDonald, L. R. Evangelista, E. K. Lenzi and G. Barbero, *J. Phys. Chem. C*, 2011, **115**, 7468.
40 K. Kunal, C. G. Robertson, S. Pawlus, S. F. Hahn and A. P. Sokolov, *Macromolecules*, 2008, **41**,7232.
41 A. S. Shaplov, D. Ponkratov, P. Vlasov, E. Lozinakaya, L.V. Gumileva, C. Surcin, M. Morcrette, M. Armand, P. H. Aubert, F. Vidal and Y.S. Vygodskii, *J. Mat. Chem. A* , 2015, **3**, 2188.
42 1 J. Dudowicz. K. F. Freed and J. F. Douglas, *J. Phys. Chem. B*, 2005, **109**, 21285.
43 J. C. A. Maxwell, *Treatise of Electricity & Magnetism*, Dover, New York 1954, pp 310-314.
44 J. Leys, R. N: Rajesh, P. C. Menon, C. Glorieux, S. Longuemart, P. Nockemann, M. Pellens and K. Binnemans, *J. Chem. Phys.*, 2010, **133**, 034503.
45 M. Watanabe, S. Nagano, K. Sanui and N. Ogata, *Solid State Ionics*, 1988, **911**, 28.
46 K. Hayamizu, E. Akiba, T. Bando and Y. Aihara, *J. Chem. Phys.*, 2002, **117**, 5929.
47 R. C. Agrawal, R. Kumar and R. K. Gupta, *Mat. Sci. Eng.*, 1998, **B57**, 46.
48 G. A. Niklasson, A. K. Jonsson, M. Stromme, Y. Barsoukova and J. R. MacDonald (Eds) In *Impedance Spectroscopy* 2nd ed., Wiley, New York, 2005, pp 302-326.
49 H. J. Schütt, *Solid State Ionics*, 1994, **505**, 70.
50 H. J. Schütt and E. Gerdes, J. Non-Cryst. Solids, 1992, 144, 1.
51 R. Coelho, *Physics of Dielectrics*, Elsevier Scientific Publishing Company, New York, 1979, pp 97-102.
52 T.M.W.J. Bandara, M.A.K.L. Dissanayake, O. A. Ileperuna, K. Varaprathan, K. Vignarooban and B.-E. Mellander, *J. Solid State Electrochem.*, 2007, **10**, 461.
53 E. M. Trukhan, *Sov. Phys. Phys. Solid State (Engl. Transl.)*, 1963, **4,** 2560.
54 T. S. Sorensen, R. Díaz-Calleja, E. Riande. J. Guzman and A. Andrio, *J. Chem. Soc. Faraday Trans.*, 1993, **93**, 2399.